Separation Science and Technology
Publication details, including instructions for authors and subscription information:
http://www.informaworld.com/smpp/title~content=t713708471

Physicochemical Characterization of Granular Ferric Hydroxide (GFH) for Arsenic(V) Sorption from Water

B. Saha[a]; R. Bains[a]; F. Greenwood[a]
[a] Advanced Separation Technologies Group, Department of Chemical Engineering, Loughborough University, Leicestershire, United Kingdom

To cite this Article Saha, B. , Bains, R. and Greenwood, F.(2005) 'Physicochemical Characterization of Granular Ferric Hydroxide (GFH) for Arsenic(V) Sorption from Water', Separation Science and Technology, 40: 14, 2909 — 2932
To link to this Article: DOI: 10.1080/01496390500333202
URL: http://dx.doi.org/10.1080/01496390500333202

Separation Science and Technology, 40: 2909–2932, 2005

ISSN 0149-6395 print/1520-5754 online
DOI: 10.1080/01496390500333202

Physicochemical Characterization of Granular Ferric Hydroxide (GFH) for Arsenic(V) Sorption from Water

B. Saha, R. Bains, and F. Greenwood
Advanced Separation Technologies Group, Department of Chemical Engineering, Loughborough University, Leicestershire, United Kingdom

Abstract: Physical and chemical characterization of granular ferric hydroxide (GFH) [e.g., scanning electron micrographs (SEM), X-ray diffraction (XRD) analysis, Brunauer-Emmett-Teller (BET) and Langmuir surface area measurements, pore size distribution, pH titration, and zeta potential measurements] were conducted to determine its performance as an adsorbent for trace arsenic(V) removal. Speciation diagrams for arsenate and phosphate were produced for the present system. The equilibrium adsorption isotherms were measured over initial arsenate concentrations ranging from 100–750 μg/L and the pH range of 4–9. The adsorption of arsenate was found to decrease as the pH of the solution was increased, thus giving the optimal adsorption of arsenate onto GFH at pH 4. Adherence to the Langmuir isotherm was found at all pHs for the arsenate adsorption. The competitive effect of phosphate on the uptake of arsenate at pH 4 by GFH was investigated, outlining the greater affinity of GFH for arsenate adsorption compared to phosphate. The kinetic performance of GFH was assessed and the results were analyzed by applying a particle diffusion model.

Keywords: Arsenic and phosphorus adsorption, granular ferric hydroxide, characterization, speciation diagram, sorption studies, kinetic studies, particle diffusion model

Received 16 May 2005, Accepted 25 August 2005
Address correspondence to B. Saha, Advanced Separation Technologies Group, Department of Chemical Engineering, Loughborough University, Leicestershire, LE11 3TU, United Kingdom. Fax: +44-(0)1509-223923; E-mail: b.saha@lboro.ac.uk

INTRODUCTION

Arsenic is present naturally within the earth's crust, held within igneous and sedimentary rocks, causing its profile to be raised to the twentieth most abundant material in the earth's crust (1). Its presence has also been increased through the use of arsenical pesticides, mining, and burning of fossil fuels. Arsenic has received widespread attention in recent times due to its toxic and carcinogenic properties. More than 13 million people in the United States routinely obtain water from public sources that have more than 10 parts per billion (ppb or $\mu g/L$) of arsenic, according to U.S. Environmental Protection Agency (USEPA) figures. Other nations have a significant problem with arsenic poisoning. Bangladesh, for example estimates between 35 and 77 million of its 125 million citizens are at risk of drinking contaminated water, where local populations are routinely exposed to arsenic poisoning through the ingestion of groundwater and eventual release into the bloodstream (2). Due to instances of arsenic presence in some parts of the United States, the USEPA has lowered the current U.S. drinking water maximum contaminant level (MCL) for arsenic to $10\,\mu g/L$ from a proposed level of $50\,\mu g/L$ (3). The European Union has issued a directive to reduce the arsenic threshold from $50\,\mu g/L$ to $10\,\mu g/L$ (4). The new limit has generated research in the United Kingdom, as 30 treatment works will be required to take some measures to reduce the arsenic level down to $10\,\mu g/L$.

Dissolved arsenic in water essentially exists as As(V) and As(III), i.e., arsenate and arsenite, respectively. Thus in order to meet upcoming legislation, increased importance has been placed on the removal of As(V) and As(III) oxyanions and oxyacids from water. The occurrence and distribution of these two forms of arsenic is largely influenced by pH and the redox conditions of the environment in which they exist. In atmospheric and slightly oxidizing environments, As(V) is the predominant species mainly as $H_2\ AsO_4^-$ and $HAsO_4^{2-}$. As a general rule, As(III) is more likely to be found in anaerobic groundwater, while arsenate, As(V), is found in aerobic surface water. Dissolution from the solid phase results in arsenolite (As_2O_3), arsenic oxide (As_2O_5) and realgar (As_4S_4) (5). Arsenate is more readily removed from water than arsenite, as it is an ionic species in the pH range typically found in the aquatic environment. Arsenite does not readily oxidize to arsenate if the pH is less than 10 without the presence of additional oxidizers (6). Arsenic can occur in four oxidation states in water, although it is usually found in the trivalent (arsenite) and pentavalent (arsenate) forms. The toxicity of arsenic compounds is as follows: arsine $>$ arsenite $>$ arsenate $>$ alkyl arsenic (7, 8).

The present study is primarily concerned with the removal of arsenate from water through sorption mechanism. The removal of arsenic from water systems has been carried out by several conventional methods, which include removal by coagulation with ferric salts, results in residual arsenic concentrations below $10\,\mu g/L$; lime softening for removal of As(V); conventional iron-manganese removal processes; ion exchange; reverse osmosis; and

adsorption onto activated alumina. A number of arsenic removal technologies have been investigated in the laboratory and for field-scale testing for the removal of trace arsenic (9–25).

The use of granular ferric hydroxide (GFH) as an efficient arsenic adsorbent was developed at the Technical University of Berlin (Germany) (9). Pal (10) indicated that a granular activated ferric oxide or ferric hydroxide should have a higher capacity for the adsorption of arsenic from water than activated alumina in a fixed-bed system, the most commonly used set up for water treatment. Thus the aim of applying GFH to arsenic removal is to combine the advantages of the widely used coagulation-filtration techniques; high removal efficiency with a small residual mass together with the fixed-bed adsorption on activated alumina.

The purpose of this work is to observe the effect on the sorption of arsenate onto granular ferric hydroxide (GFH). The physical and chemical characterization of GFH in the form of scanning electron micrographs (SEM), X-ray diffraction (XRD) analysis, Brunauer-Emmett-Teller (BET) and Langmuir surface area measurements, pH titration, and zeta potential measurements have been conducted to determine its performance as a sorbent for As(V) removal. Density functional theory (DFT) has been used to analyze the pore size distribution data. The speciation diagrams of arsenate and phosphate have been produced to interpret the underlying sorption mechanism. The sorption of arsenate from aqueous solution onto GFH has been studied in batch equilibrium experiments. The influence of pH on arsenate sorption capacity has been examined. The kinetic performance of GFH has been assessed and the results have been analyzed by applying a particle diffusion model. The competitive effect of phosphate on the uptake of arsenate by GFH has also been investigated.

EXPERIMENTAL

Adsorbent Material—Granular Ferric Hydroxide (GFH)

The granular ferric hydroxide used in this study was supplied by GEH, Wasserchemie, Germany. The sample was produced from ferric chloride solution by neutralization and precipitation with sodium hydroxide. Sodium hydroxide and ferric chloride were contacted at 313 K. The resulting precipitate was washed, passed through a membrane, and then stored in plastic tubs. The tubs were conditioned in situ with a solid content as low as 15%, then left to naturally dewater, until the volume was replaced by 75%. The equilibrium pH of the product was 7. GFH is a poorly crystallized β-FeOOH, which resembles the mineral Akaganeit, containing chloride, which aids the structure of adsorbent. The pores of the GFH are completely filled with water leading to a high density of available adsorption sites and therefore a high adsorption capacity. The characteristics of GFH are given in Table 1.

Table 1. Characteristics of GFH

Characteristics	Value
Moisture content, %	43.3
Specific surface area, m^2/g	250–350
Density of grain, g/cm^3	1.59
Bulk density, g/cm^3	1.32
Porosity of grains, %	75–80
Bulk porosity, %	26
Active substance: $Fe(OH)_3$ and (am-FeOOH), %	55
Water content, %	46

Chemicals and Materials

Arsenate solutions were prepared using $Na_2AsO_4 \cdot 7H_2O$ and was supplied by Fisons; phosphate solution were prepared using Na_2HPO_4 (Sigma). Sodium hydroxide solution was prepared by using laboratory-grade pellets supplied by Fisher Scientific, UK. Standard solutions of sodium hydroxide, hydrochloric acid, and palladium modifier (palladium nitrate, 10 wt% solution in 10 wt% nitric acid) were obtained from Fisher Scientific, UK. The analytical reagents used for the colorimetric method for phosphate determination were ammonium molybdate and L-ascorbic acid (purchased from Fisons) and antimonyl potassium tartrate and concentrated sulphuric acid (both from Fisher Scientific, UK).

Analyses of Arsenate and Phosphate

The concentration of arsenic present in the sample was analyzed using a Varian Graphite Furnace Atomic Absorption (AA), GTA 100. A palladium modifier was used to permit the use of a higher ashing temperature and to enhance the analyte signal. The calibration procedure followed in this work is as follows. A standard arsenate solution of 75 μg/L was made up from 1000 mg/L standard arsenic solution. The palladium modifier solution consisted of 0.1% palladium and 0.25% citric acid; this was made from a 10 wt% solution and 10 wt% nitric acid of palladium nitrate and citric acid. The total volume of the 75 μg/L sample being injected into the GTA was set to 30 μL, consisting of 12 μL standard, 11 μL palladium modifier and 7 μL deionized water. The GTA lamp was set to a current of 10 mA, a slit width of 0.5 nm, and a wave length of 193.7 nm. The carrier gas (argon) was set to a flow rate of 3 L/min.

Phosphate analysis was carried out using a colorimetric method, with the aid of a Perkin Elmer Lambda 12 dual beam UV/VIS spectrophotometer at a wave length of 882 nm. In order for the phosphate analysis to be carried out,

a reagent was prepared as follows: 125 mL of sulphuric acid (5 N), made from a standard solution of 18 M and mixed with 37.5 mL of ammonium molybdate (20 g in 500 mL) in a glass flask. A total of 75 mL of 0.1 M ascorbic acid and 12.5 mL of potassium antimonyl tartrate (1 mg/mL) were added and thoroughly mixed. A new reagent was prepared for each batch of samples, as degradation occurs after more than 24 h. Therefore, a new calibration curve was required for each run and the R^2 values were always greater than 0.99. To determine whether there was a time effect on absorbance values, the samples were reanalyzed after 15 min. The difference between the two reading for several samples across the concentration range used was less than 4%.

A calibration was then produced, using calibration standards of 25, 50, 100, 150, 250, and 500 ppb that were prepared using the following method. A 4 mL volume of the phosphorus solution was placed into a 100 mL volumetric flask, 4 mL of the reagent was added, and the solution volume made up using deionized water. This was left for 10 min for the complexation reaction to occur.

A back correction was made to the sample absorbance using a blank at each measurement; the calibration was then carried out using the spectrophotometer. A cuvette was filled with the sample and the absorbance measured at 882 nm. A plot of log absorbance vs. log concentration, i.e., $\log(A_{882})$ vs. $\log(C_p)$ was constructed and the equation of the line of best fit determined, according to Eq. (1).

$$\log(A_{882}) = m \log(C_p) + c \tag{1}$$

where

$\log(A_{882})$ = log absorbance at 882 nm
m = gradient of the line
$\log(C_p)$ = phosphate concentration (μg/L)
c = intercept

The unknown phosphorus concentration was calculated using Eq. (2).

$$C_p = 10^{[\{\log(A_{882}) - c\}/m]} \tag{2}$$

Physicochemical Characterization Procedure

Scanning Electron Micrography (SEM)

Scanning Electron Micrographs (SEM) were taken on a Cambridge Instrument stereo scan 360 microscope at room temperature. The normal second electron mode (i.e., not back scattering) was used and the accelerating voltage was set to 10 kV. Prior to analysis, the GFH sample was dried in a vacuum oven at room temperature, then mounted using PVA glue on an aluminium platform and gold coated.

XRD Analysis

A Philips PW1050 goniometer with a copper X-ray tube was used. A graphite monochromator with a 1° scatter slit and a 0.2 mm receiving slit was added. A Hilton Brooks nucleonics and automation system was used. Prior to analysis, GFH sample was dried in a vacuum oven at room temperature. The crushed GFH sample passed into an aluminium holder. XRD scans were carried out in the range 10–80° at 0.05° step size and 0.2°/min.

Surface Area and Pore Size Distribution Analysis

Surface area and porosity measurements were carried out by nitrogen adsorption and desorption methods using a Micromeritics ASAP 2010 automatic analyzer fitted with an optional high-stability $133.3\,N \cdot m^{-2}$ pressure transducer. Weighed sample of GFH was prepared by out-gassing for a minimum period of 24 h at 373 K on the degas ports of the analyzer. Adsorption isotherms were generated by dosing nitrogen (>99.99% purity) onto the adsorbent contained within a bath of liquid nitrogen at approximately 77 K. Surface area was measured for linear relative pressure range between 0.05 and 0.15.

pH Titration

A number of samples were prepared by measuring 10 mL 0.1 M sodium nitrate to a series of 25 mL flasks. Nitrate was used as an electrolyte as Fe(III) complexes are less likely to form. Different initial pH values were obtained by addition of 0.1 M NaOH or 0.1 M HNO_3 solutions. A total solution volume of 15 mL was maintained by addition of deionized water, to ensure the adsorbent weight to solution volume ratio was kept constant. Prior to the addition of the GFH adsorbent, the pH of the solution was measured by a Mettler Toledo 340 pH meter calibrated at pH 4 and pH 10. Total solution volume used was 15 mL per 25 mg dry sample. The samples were shaken for 2 days on an arm shaker at 298 ± 1 K. At the end of the experiment, the pH of the supernatant solution was measured by a Mettler Toledo 340 pH meter.

Zeta Potential Measurements

Zeta potential of the materials in the size range 0–45 μm was measured using a Malvern Zetamaster instrument. The measurements were based on a Laser Doppler Electrophoresis technique (27). The technique operates by measuring the interference fringes of two laser beams at the point where the beams cross. Particles that cross the beams will cause the interference fringes to shift, and this can be related back to the particle's velocity and hence to the electrophoretic mobility. This technique offers several advantages over traditional microscopic methods. It averages the measurement over thousands of readings, generating an intensity distribution, greatly reducing statistical

errors. Very low or zero zeta potential can also be measured accurately by virtue of an optical modulator which causes a Doppler shift in one of the beams.

The zeta potential of GFH samples was determined using the same samples that were prepared for pH titration. The zeta potential of each solution was measured after the equilibration had been attained. The measurement was conducted at 298 ± 1 K. 5 mL of the supernatant material were collected using a plastic Luer syringe that resulted in an optimum count rate of 4000 counts/sec. The suspension was injected into a quartz cell in an electrophoresis chamber.

Batch Adsorption Studies

Single Component Studies

A 1 L stock solution of 20,000 μg/L As(V) was prepared by dissolving sodium arsenate ($Na_2HAsO_4 \cdot 7H_2O$) in deionized water. The required concentration of As(V) was prepared in a 2 L volumetric flask using the stock solution, then split into four samples of 490 mL decanted into 500 mL Nalgene bottles. The remaining solution was kept in a volumetric flask for future reference. Adsorption experiments were carried out in the pH range 4–9, sample pH was adjusted using 0.1 M HCl or 0.1 M NaOH prepared from standard 1 M solutions. A mass of 5 mg of GFH was added into each of the bottles. The GFH was weighed on a Metttler AJ100 balance within the accuracy limit of ±0.0005 g.

The sample bottles were placed into a C25 incubated orbital shaker (New Brunswick Scientific) for 24 h at 298 ± 1 K, the pH was measured using a Mettler Toledo 340 pH meter maintained at its initial value throughout the experiment by addition of stock acid or alkali. Any addition of acid/alkali to the solution volume was noted and was <0.5% of the total batch volume. The experiment was carried out at pH values of 4, 5, 7, and 9 and at different As(V) concentrations. It was assumed that the solution had reached equilibrium when there was no change in the solution pH. After this period, a 5 mL sample of the mixture was extracted and analyzed for As(V) content.

Binary Component Studies

The binary component analysis was carried out based on the combined adsorption effects of phosphate(V) and As(V) on the GFH adsorbent. A 245 mL sample of 150 μg/L As(V) solution was placed into a Nalgene bottle, along with 245 mL of the equivalent molar amount of phosphate solution. A mass of 5 mg of GFH was added to the sample and the pH was adjusted to 4 using 0.1 M HCl. The sample bottles were placed into a C25 incubated orbital shaker (manufactured by New Brunswick Scientific) for 24 h at 298 ± 1 K, the pH was also maintained at its initial value by

addition of acid or alkali. The solution pH was measured using a Mettler Toledo 340 pH meter. Any addition of acid/alkali to the solution volume was noted and was $<0.5\%$ of the total batch volume. Then the samples were analyzed for As(V) and phosphate following the method described in the analyses section.

Kinetic Studies

The kinetic studies were performed at As(V) concentrations of 100 μg/L using GFH. The samples were sieved into two fractions, i.e., 75–180 μm and 600–700 μm. A 500 mL sample of the As(V) solution was prepared at pH 4 and placed into the glass reactor vessel suspended in a water bath at a temperature of 298 K. The solution was agitated by an impellor revolving at 500 rpm. Once the solution temperature had reached a constant temperature of 298 K, a known quantity of previously wetted GFH sample was added to the reactor. This was noted as the starting time of the experiment. The samples were collected at various time intervals and then analyzed for As(V) content by Graphite Furnace Atomic Absorption. All kinetic experiments were conducted for 3 h and repeated twice for precision and accuracy.

RESULTS AND DISCUSSION

Speciation

Construction of speciation diagrams for each pollutant studied is important in determining the nature of the ions present in solution. Speciation is dependent on the total solute concentration and the solution pH. The charge of a species (anionic, cationic, or neutral) affects the removal capacity of the adsorbent. At low pH, the GFH surface is positively charged, hence will attract anions and at high pH the surface is negatively charged and will attract cations. Hence, it is essential to produce the speciation diagram of each species studied.

Arsenic(V) Speciation

The speciation of As(V) is important in determining the chemistry behind aqueous arsenic solutions, thus enabling treatment methods for removing dissolved arsenic from water to be established. The distribution of As(V) compounds are influenced by pH; this can be shown by a speciation diagram and will give the predominant form of As(V) present at a given value of pH. Thus the method of removing arsenic can be determined by using the diagram to find out the predominant species present at a known pH of aqueous solution. The arsenate ion, AsO_4^{-3} is a commonly found

species of arsenic present in water. Arsenic(V) as it is otherwise known exists in four forms in aqueous solution: H_3AsO_4, $H_2AsO_4^-$, $HAsO_4^{2-}$, and AsO_4^{3-}. The predominant species of arsenic(V) present varies with the pH of the solution. The diagram is constructed from the equilibrium expressions, where K is the equilibrium constant for the equilibrium reaction of each As(V) species, and then equations are formed where each species is expressed as a function of pH and total arsenic concentration only. The equations for As(V) dissociation in water are given as follows (11):

Equilibrium Expressions

$$H_3AsO_4 \Longleftrightarrow H^+ + H_2AsO_4^-$$

$$K_1 = \frac{[H^+][H_2AsO_4^-]}{[H_3AsO_4]} \quad \mathrm{pK}_1 = 2.2 \tag{3}$$

$$H_2AsO_4^- \Longleftrightarrow H^+ + HAsO_4^{2-}$$

$$\mathrm{K}_2 = \frac{[\mathrm{H}^+][\mathrm{HAsO}_4^{2-}]}{[\mathrm{H}_2\mathrm{AsO}_4^-]} \quad \mathrm{pK}_2 = 6.98 \tag{4}$$

$$\mathrm{HAsO}_4^{2-} \Longleftrightarrow H^+ + AsO_4^{3-}$$

$$K_3 = \frac{[H^+][AsO_4^{3-}]}{HAsO_4^{2-}} \quad \mathrm{pK}_3 = 11.6 \tag{5}$$

The total arsenic concentration is therefore the sum of the four arsenic(V) species:

$$[\mathrm{As}] = [\mathrm{H_3AsO_4}] + [\mathrm{H_2AsO_4^-}] + [\mathrm{HAsO_4^{2-}}] + [\mathrm{AsO_4^{3-}}] \tag{6}$$

For each species, the variation in concentration with pH can be calculated by choosing a total arsenic concentration value and substituting in the values for the equilibrium constants K_1, K_2, and K_3.

The pH is related to the concentration of H^+ ions by the following expression:

$$\mathrm{pH} = -\log_{10}[\mathrm{H}^+] \tag{7}$$

Therefore by varying the value of pH, the concentration of H^+ ions used in the previous expressions can be varied. The total arsenic concentration is kept constant and the concentration of each species for each pH is then calculated as a fraction of the total concentration value. Taking an arsenic concentration of 400 μg/L, this can then be converted into mol/L by dividing by the atomic mass of arsenic, to give a total arsenic concentration of $[\mathrm{As}] = 5.34 \times 10^{-6}$ mol/L. The constants can then be substituted into expressions for each of the four arsenic(V) species concentrations at different pH values to give the speciation diagram for As(V) as shown in Fig. 1.

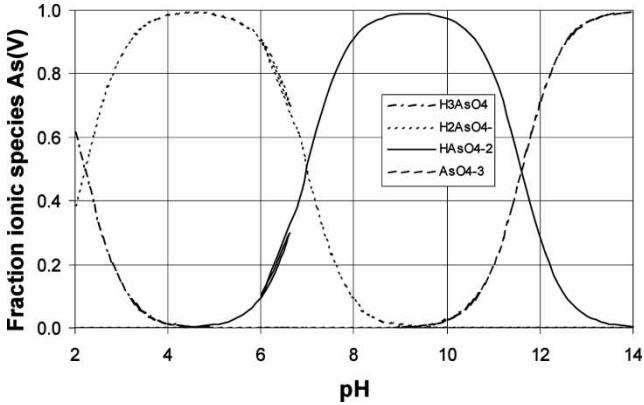

Figure 1. Arsenate speciation diagram showing the predominate species present at each pH.

Phosphate(V) Speciation

The principal sources of phosphates in natural waters are the apatite minerals, $3Ca_3(PO_4)_2 \cdot CaF_2$ and $3Ca_3(PO_4)_2 \cdot CaCl_2$, which dissolve in aqueous solution to $H_2PO_4^-$, HPO_4^{2-}, and PO_4^{3-}. The predominant species of phosphate present varies with the pH of the solution. A speciation diagram is a representation of the predominant form of phosphate for a given value of pH. The dissociation of orthophosphoric acid in water indicates a molecular dispersion as H_3PO_4, which ionizes by the following equilibrium expressions used to construct the speciation diagram (26) where K is the dissociation constant for the equilibrium reaction of each phosphate species being ionized. Equations can then be formed where each species is expressed as a function of pH and total phosphorus concentration only. The equilibrium expressions are shown:

Equilibrium Expressions

$$H_3PO_4 \Longleftrightarrow H^+ + H_2PO_4^-$$

$$K_1 = \frac{[H^+][H_2PO_4^-]}{[H_3PO_4]} \quad \mathrm{pK}_1 = 2.1 \tag{8}$$

$$H_2PO_4^- \Longleftrightarrow H^+ + HPO_4^{2-}$$

$$K_2 = \frac{[H^+][HPO_4^{2-}]}{[H_2PO_4^-]} \quad \mathrm{pK}_2 = 7.2 \tag{9}$$

$$HPO_4^{2-} \Longleftrightarrow H^+ + PO_4^{3-}$$

$$K_3 = \frac{[H^+][PO_4^{3-}]}{HPO_4^{2-}} \quad \mathrm{pK}_3 = 12.2 \tag{10}$$

The total phosphorus concentration is therefore the sum of the four phosphate species:

$$[P] = [H_3PO_4] + [H_2PO_4^-] + [HPO_4^{2-} + [PO_4^{3-}] \quad (11)$$

For each species the variation in concentration with pH can be calculated by choosing a total phosphorus concentration value and substituting in the values for the equilibrium constants K_1, K_2, and K_3. The pH is related to the concentration in H^+ ions as shown in Eq. (7). Therefore by varying the value in pH, the concentration of H^+ ions used in Eq. (7) can be varied. The total phosphorus concentration is kept constant and the concentration of each species for each pH is then calculated as a fraction of the total concentration value. Taking a phosphorus concentration of 500 μg/L, this can then be converted into mol/L to give an total phosphorus concentration, $[P] = 1.61 \times 10^{-5}$ mol/L. The constants can then be substituted into expressions for each of the four phosphorus species concentrations at different pH to construct the speciation diagram as shown in Fig. 2.

Physicochemical Characterization

Scanning Electron Micrography (SEM)

Figures 3a and b show micrographs of the GFH particles and particle surface, respectively. GFH is a poorly crystallized β-FeOOH, which resembles the mineral Akaganeit containing chloride. The average particle size (diameter) is quite large, 500–650 μm. The structure appears to be robust and without

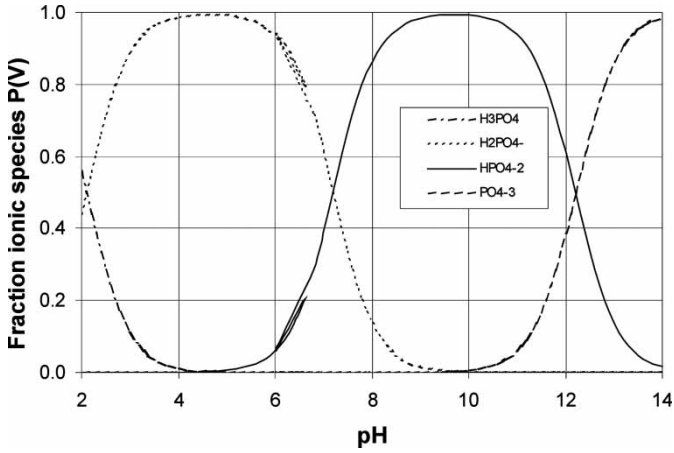

Figure 2. Phosphate speciation diagram showing the predominate species present at each pH.

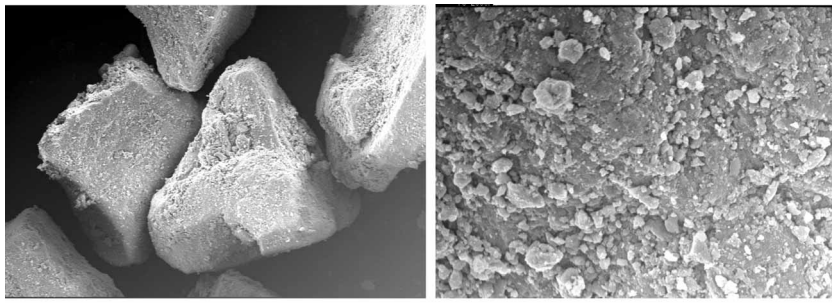

(a) (b)

Figure 3. Scanning Electron Micrograph (SEM) of GFH (a) particles, (b) particle surface.

agglomerated material (see Fig. 3a). The surfaces of the GFH sample (Fig. 3b) appear rough due to the presence of fine particles attached to the larger grain surfaces.

Surface Area and Pore Size Distribution Analysis

Surface area and pore size distribution analysis for all samples were carried out by N_2 adsorption/desorption method at 77 K (27). The Density Functional Theory (DFT) model is recognized as a powerful tool for studying inhomogeneous classical fluids (28, 29). Hence, porosity distribution of the GFH was calculated using the DFT model based on nitrogen adsorption, assuming slit pore geometry.

The calculation method requires the solution of a system of complex integral equations that are implicit functions of the density vector. Since analytical solutions are not possible, the problem has been solved using iterative numerical methods. The complete details of the theory and mathematical formulations have been described by Oliver (28). Inversion of the integral equation of adsorption to determine micropore size distribution from experimental isotherms using the DFT model usually produces results showing minima near 6 and 10 Å effective pore width, regardless of the simulation method used. This is assumed to be a model-induced artifact (27). The inclusion of surface heterogeneity in the model, while more realistic, does not change this observation significantly. The strong packing effects exhibited by a rigid parallel wall model seem likely to be the dominant feature causing the double minima in the derived pore size distributions.

Brunauer-Emmett-Teller (BET) and Langmuir surface areas of GFH sample are 351 and 253 $m^2\ g^{-1}$, respectively. The sample has a comparable surface area to that of Deliyanni et al. (30). They produced Akaganeite material at room temperature with a specific surface area of 330 $m^2\ g^{-1}$. However, this material was nanocrystalline, which could account for the

high specific surface area. Crosby et al. (31) reported the BET surface area of a number of ferric hydroxide materials, all in the range of $160-230\,m^2\,g^{-1}$ and were classified as an amorphous material, am-FeOOH. It is a general observation that the higher the degree of crystallinity, the lower the specific surface area.

The adsorption isotherm of the GFH sample is shown in Fig. 4. The isotherm describes that the adsorption for GFH can be used to calculate specific surface area of the material and the pore size distribution. During the adsorption process, the adsorbate molecule diffuses through the pores of the solid. Initially this is through the smallest pores or micropores. These sites have the greatest energy and have the greatest polarity. As the pressure increases, the adsorbate molecules diffuse to larger and hence the less energetic pores. A small pressure difference is required when nitrogen is adsorbed onto the surface. On desorption, however, a higher pressure difference is required to enable the nitrogen to desorb back into the micropores. Figure 5 indicates that GFH has a high percentage of microporosity as the isotherm shows substantial quantity of adsorbed nitrogen in the initial portion of the isotherm. However, the isotherm is a characteristic of mesoporous substances, where capillary condensation occurs. A bottleneck effect between micropores and mesopores causes adsorbate condensation to occur. The quantity of micropores could be related to the pH control during the production of the material. The pH of GFH sample was controlled to a constant value throughout the reaction procedure. At higher relative pressure, the

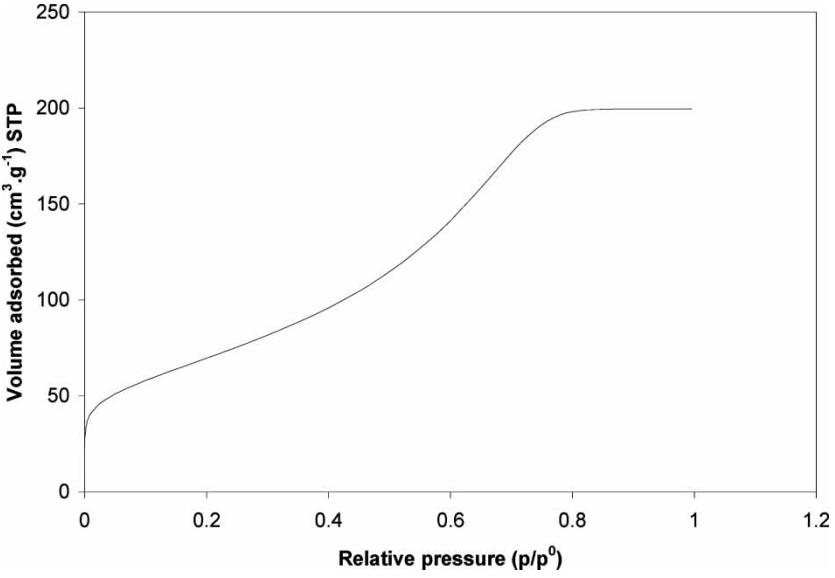

Figure 4. Adsorption isotherm of GFH sample.

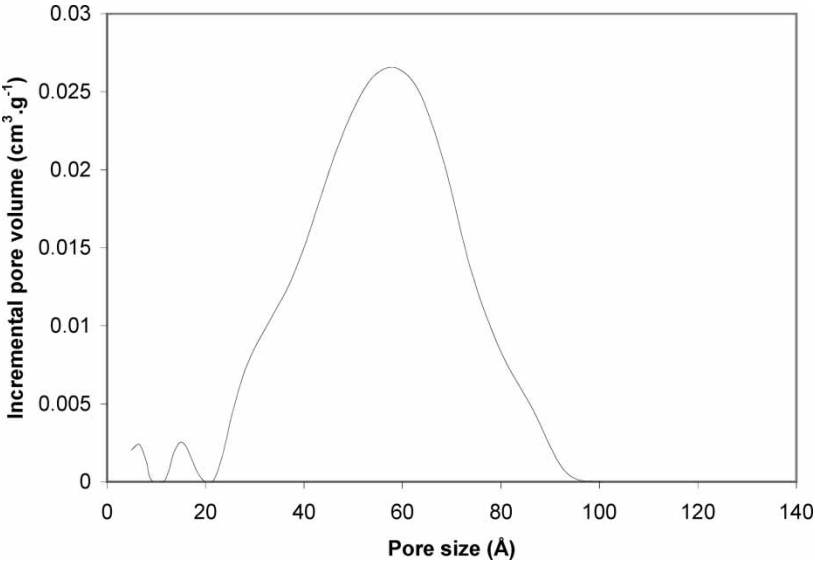

Figure 5. DFT pore size distribution of GFH sample.

isotherm flattens up, which indicates the absence of macroporosity in the sample. Hence from the adsorption isotherm it can be concluded that GFH sample is mainly mesoporous. Density Functional Theory (DFT) pore size distribution results are shown in Fig. 5. The results suggest that the GFH sample contains a significant amount of mesoporosity.

pH Titration, Zeta Potential, and XRD Analyses

The values of point of zero net proton charge (PZNPC) and iso electric point (IEP) for GFH were found to be 5.7 and 7.5, respectively. The zeta potential results indicate the amphoteric nature of GFH, with an approximately equal amount of positive and negative surface charge across the pH range. At pH $>$ IEP, the GFH surface will attract cations from the surface, conversely at pH $<$ IEP it will attract anions. The IEP is an indication of external surface charge only; however, the PZNPC takes into account both the external and internal charges. The difference between PZNPC and IEP for GFH sample is -1.8. This indicates that the internal surface is more negatively charged than the external surfaces. The residual chloride content in the GFH would also reduce the PZNPC. Moreover, the surface area and pore structure may affect the balance of external and internal charges.

The XRD output of GFH shows considerable amount of crystallinity in the material. It is also evident from the result that GFH sample is not pure as there was a peak associated with hematite (33°) that was identified by XRD analysis. The time of aging the precipitate can be a contributing factor

to increased crystallinity. The crystallinity increases with the increase in the time of aging. It was also determined that chloride content of GFH sample is 0.60 mmol/g and the equilibrium pH in water in about 3.9. The quantity of chloride present in GFH affects the XRD output of the sample, a lower chloride content causes peak broadening. The presence of chloride in the GFH sample is attributed to a lesser degree of washing of the sample and hence residual chloride from the reaction may still be bound within the structure. The small pore size of GFH sample indicates the inhibition of chloride removal. The residual chloride slowly leaches out from the material as HCl, hence the equilibrium pH of GFH in water is about 3.9. This is comparable with the equilibrium pH of Akaganeite, i.e., 3.5.

Equilibrium Study

Arsenic(V) adsorption experiments were carried out at each pH value in the range 4–9 for GFH sample. The amount of arsenate present in the sample for each concentration and pH was taken to be the equilibrium concentration (C_{eq}), in μmol/L. The results for each value of pH were then plotted on a graph of the amount of arsenate adsorbed per g of GFH (q) *vs.* the equilibrium concentration of arsenic (C_{eq}) (see Fig. 6). The adsorption capacity (q) is calculated from Eq. (12)

$$q = (C_o V_o - C_{eq} V_{eq})/m \tag{12}$$

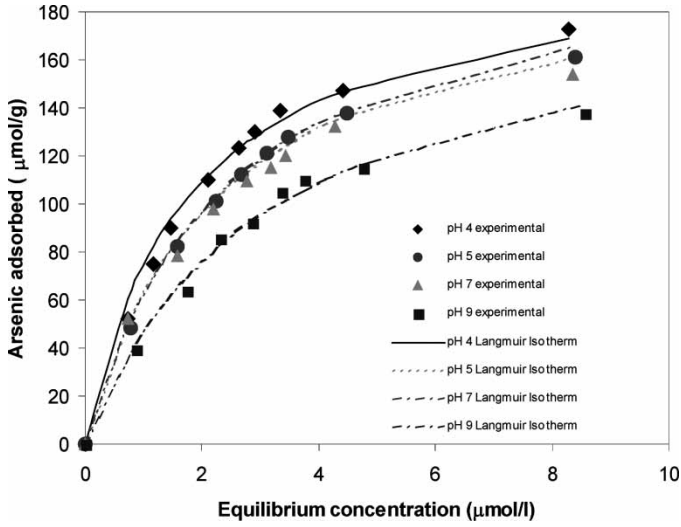

Figure 6. Arsenic uptake by GFH (pH range 4–9).

where, q = adsorption capacity (μmol/g); C_o = initial concentration (μmol/L); V_o = initial volume of solution (L); C_{eq} = equilibrium concentration (μmol/L); V_{eq} = equilibrium volume (L); m = mass of adsorbent (g).

In order to make a comparison with a theoretical model the results were then used to plot a Langmuir isotherm, as this had been shown to fit to the adsorption of arsenate onto GFH by Pierce and Moore (12) and Thirunavukkarasu et al. (32). The expression for Langmuir Isotherm model is given in Eq. (13)

$$q = \frac{q_{max} C_{eq}}{k_L + C_{eq}} \tag{13}$$

where, q_{max} = maximum adsorption capacity (μmol/g); k_L = Langmuir constant.

Thus the maximum amount of arsenate adsorbed per g of GFH at each pH can be determined as shown in Table 2. The experimental results of the adsorption of arsenate onto GFH shows adherence to the Langmuir adsorption isotherm with initial concentrations of arsenate ranging from 100 μg/L up to 750 μg/L. For As(V) removal, Thirunavukkarasu et al. (32) estimated the adsorption maxima and the adsorption density at a residual concentration of 5 μg As/L using Langmuir model and the reported values are 159 and 32 μg As/g GFH, respectively. Their estimated adsorption density was lower than the value reported by Driehaus et al. (9) and Fuller et al. (33). Driehaus et al. (9) reported that at a residual As(V) concentration of 10 μg/L, the adsorption density of GFH was 1 mmol As/g Fe, at high initial As(V) concentration. They also reported that arsenate adsorption on freshly prepared ferric hydroxide was higher than the adsorption on GFH. It is expected that at a high initial As concentration or at a high As/Fe ratio, the adsorption maxima and adsorption density will also be high. The amount of arsenate adsorbed per g of GFH decreases when the pH increases from pH 4 to pH 9, as would be expected for anion exchange. For the present work, the highest amount of arsenate adsorbed is 170 μmol/g, at pH 4 at an initial concentration of 400 μg/L. Driehaus et al. (9) also found for a granular ferric hydroxide that arsenate adsorption decreased with increasing pH. Similar observations were also reported

Table 2. Maximum arsenic (V) uptake capacity at different solution pH

pH	q_{max} (μmol/g)
4.0	212
5.0	208
7.0	206
9.0	192

for ferrihydrite (34) and goethite (35, 36). It is to be noted that the results are comparable with the reported data for As(V) sorption by goethite particles (36).

From the speciation diagram of arsenate (see Fig. 1), it can be seen that the most predominate species present at pH 4 is $H_2AsO_4^-$. The iso electric point (IEP) for GFH is approximately near neutral, i.e., pH 7.4. Hence at pH 4, the surface is positively charged and will attract anions. For protonated anions, such as arsenate or phosphate, ligand exchange may be accompanied by a deprotonation at the surface, resulting in a bidentate innersphere bonding (37). As the pH increases, the degree of positive surface charge decreases, lowering the attractive forces toward anionic species. Neutral adsorption occurs through proton dissociation from acid surface. Adsorbed species receive a proton from solution to equilibrate with solution. At pH $>$ IEP, there is some arsenic adsorption despite there being mutual repulsion between the negative surface and anionic species. Therefore the energy gained by the surface in forming new bonds with the anion must be greater than the repulsive forces, for any adsorption to occur. Moreover, the speciation of arsenate changes from $H_2AsO_4^-$ to $HAsO_4^{2-}$, increasing the negative charge of the species. Removal at higher pH by specific adsorption is possible, if the undissociated acid donates a proton to the surface hydroxyl group to form water that can be displaced by the anion. Arsenic acid, H_3AsO_4, dissociates to $H_2AsO_4^-$ and $HAsO_4^{2-}$ anions, which would have a greater effect on the surface charge than the singly charged $H_2AsO_3^-$ anion of arsenous acid. It is capable of coordinating to the surface atoms of the GFH allowing adsorption of the anion to occur. The proton produced is used to remove the OH^- from the coordinating layer of the surface and provide a site for the anion to attach. The ease at which a proton can be removed from the undissociated acid in solution varies with the pH of the solution (12).

The GFH surface has different types of surface sites, with differing affinities for the adsorbate ions. The surface density of the strong binding sites would be much less than the weaker binding sites, after which point the anions start to adsorb on the weaker binding sites (38). Thus, adsorption proceeds until all the strong binding sites are occupied. The underlying removal mechanism in every arsenic removal technology is ion exchange and Lewis acid-base interactions. As(V) can undergo both ion exchange (Coulombic) as well as Lewis acid-base interaction (2). The high adsorptive capacity of GFH for arsenate can be explained by the structure of the GFH, a loose hydrated structure which is permeable to hydrated ions, allowing adsorption to easily occur.

Figure 7 shows the plot of C_{eq}. *vs*. q for both arsenate and phosphate binary sorption at a pH of 4. It can be seen that both materials are easily adsorbed by the GFH. However, GFH was found to be more selective to the adsorption of arsenate compared to phosphate. Driehaus et al. (9) reported a similar observation for their studies. This result also corresponds to the

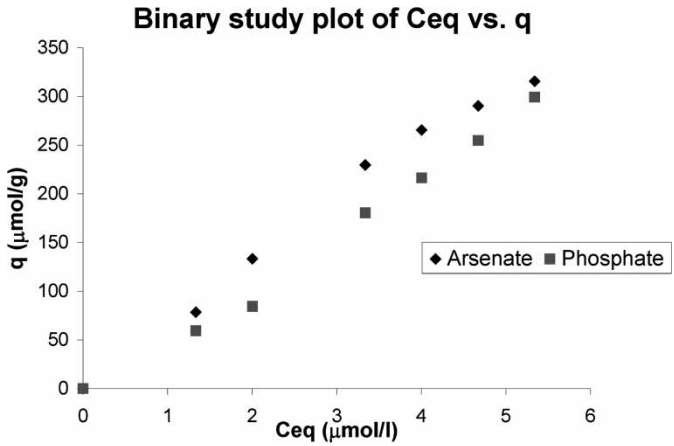

Figure 7. Binary adsorption isotherm of arsenate and phosphate at pH4.

results of Ryden et al. (39), who found a higher adsorption density of arsenate on hydrous ferric hydroxide gel with equimolar addition of arsenate and phosphate. At an equilibrium concentration of 2.45 μmol/L of phosphate the maximum adsorption capacity of phosphate per g of GFH was 125 μmol/g, a value substantially lower than that observed for arsenate sorption (175 μmol/g). It is evident that phosphate competes strongly with arsenate and hence phosphate is a major water constituent that could reduce the removal of arsenate by GFH.

The chemistry of arsenate and phosphate are similar (see Figs. 1 and 2) and it would be expected that a similar process would describe the adsorption mechanism. The overall arsenate capacity is about 40% higher than phosphate. The effective ionic radii at 298 K for both arsenic and phosphorus are approximately 4 Å. Lumsdon et al. (40) reported that the arsenate is a larger ligand than phosphate (ionic radii of arsenate and phosphate are 248 and 238 nm, respectively; As-O bond is ~10% longer than P-O bond as determined by FTIR analysis), hence arsenate interacts more strongly with hydroxyl ion (OH^-) at the surface and is preferred. It was also reported by Jain and Loeppart (41) that phosphate adsorption was lower on ferrihydrite, indicating arsenate is preferred over phosphate. This is in good agreement with the results of the present research.

Kinetic Study

Kinetic studies were conducted to examine the relationship between GFH particle size and arsenate uptake rate. The kinetics of the arsenate adsorption was studied over 3 h for two different size fractions (75–180 μm and 600–700 μm) of GFH sample (see Fig. 8). The results shown in Fig. 8

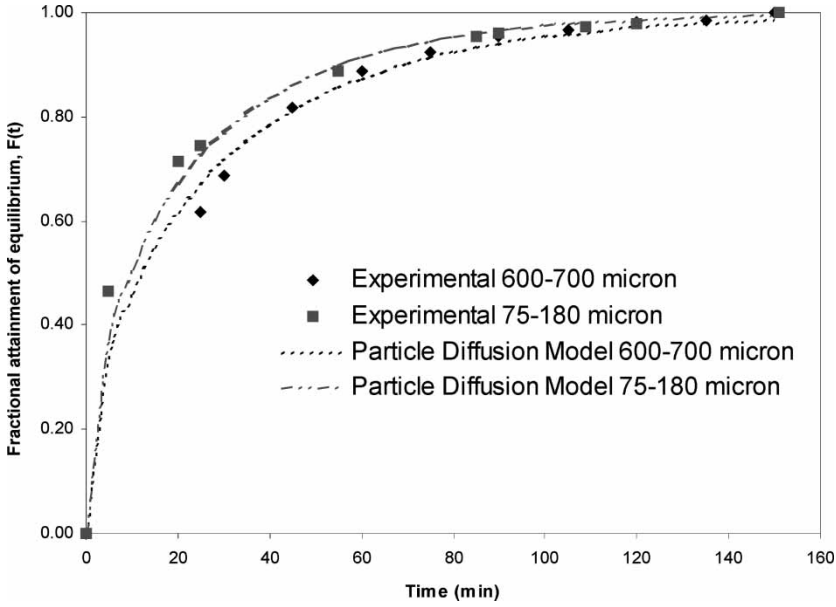

Figure 8. Arsenic(V) kinetic studies of GFH sample for two particle size fractions.

confirm that there was a significant improvement in kinetics by using smaller particle fraction of 75–180 μm. The rate of sorption of arsenate ion will depend on its mobility in the solution phase, the pore structure and the particle size of the adsorbent, and the hydrodynamics of contact between the solution and particle phase.

It is considered that the sorption of trace arsenate ions from aqueous solution by GFH is an example of reactive ion exchange. A comprehensive theoretical treatment of various reactive ion exchange processes is described by Helfferich (42). It is to be noted that kinetic studies were performed with vigorous stirring and therefore film diffusion was not a controlling factor in the sorption process. Moreover, the rate of attainment of equilibrium arsenate sorption was seen to be nearly independent of the arsenate concentration. This indicated the possibility of ordinary particle diffusion control of the sorption process. Hwang and Helfferich (43) introduced a numerical technique to extend the Nernst-Planck model for intraparticle diffusion controlled ion exchange to multispecies systems with very fast reversible reactions at local equilibrium. This method is applicable to most reactions, which are very fast compared with diffusion in ion exchange. However, the sorption of arsenate ion by GFH particle involves multiple processes, perhaps involving complex formation, which are not elucidated. Hence, an approximate and simpler model based on Fick's flux equations was used to analyze the overall rate of metal sorption.

The rate of arsenate exchange is determined by diffusion processes, the simplest case being that of isotopic exchange, which is the exchange of the arsenate species predominate and the hydroxyl ions (OH^-) in equilibrium, where most of the complicating effects are ignored but a well-established theory still exists (42). Here we assume that all the arsenate ions are initially in the GFH and that the concentration across the GFH particle surface is equal to the concentration of the bulk solution. Therefore, the resistance to diffusion across the interface is negligible. In order to compare the rate of arsenate sorption by GFH from aqueous solutions, an effective diffusion coefficient for sorption into GFH sample has been calculated by assuming particle phase control governed by Fick's second law.

The experimental kinetic results were plotted as fractional attainment of equilibrium, F(t), *vs.* time in minutes (see Fig. 8). Where F(t) was calculated from Eq. (14)

$$F(t) = \frac{\bar{Q}_A^o - \bar{Q}_A(t)}{\bar{Q}_A^o - \bar{Q}_A^\infty} \tag{14}$$

where, $\bar{Q}_A(t)$ = concentration of arsenate at time t(μmol/L); $\bar{Q}_A^o$ = initial concentration of arsenate (μmol/L); $\bar{Q}_A^\infty$ = equilibrium concentration of arsenate (μmol/L).

For practical use, applying Vermeulen's equation, fractional attainment of equilibrium can be approximated to the following equation (42)

$$F(t) \equiv \left[1 - exp\left(-\frac{\bar{D}t\pi^2}{r_o^2}\right)\right]^2 \quad 0 \le F(t) \le 1 \tag{15}$$

where, $F(t)$ = fractional attainment of equilibrium; $\bar{D}$ = effective particle phase diffusivity (cm^2/s); t = time for arsenate sorption (s); r_o = radius of the GFH particles assuming spherical geometry (cm). Thus the fractional attainment of equilibrium, $F(t)$, depends only on the magnitude of the dimensionless time parameter, $\bar{D}t/r_0^2$. The half time for arsenate sorption is given by substituting $F(t) = 0.5$, *i.e.*,

$$t_{1/2} = \frac{0.03r_o^2}{\bar{D}} \tag{16}$$

Hence, the relative rate is proportional to the diffusion coefficient in the GFH, particle and inversely proportional to the square of the particle radius. Equation (15) can be rearranged to the following equation:

$$-\ln[1 - \{F(t)\}^2] = \frac{\bar{D}\pi^2}{r_0^2}t \tag{17}$$

Hence for particle diffusion controlled mechanism, a plot of $-\ln[1 - \{F(t)\}^2]$ *vs.* t should be linear (passing through the origin) and the effective particle phase diffusivity, $\bar{D}$, can be calculated from the slope of the graph. It can be seen from Fig. 8 that the particle diffusion model fitted the experimental

Table 3. Summary of the diffusion coefficients and half times ($t_{1/2}$) for As(V) sorption for different GFH particle sizes

Particle size (μm)	Average effective particle phase diffusivity, $\bar{D}$ ($cm^2 s^{-1}$)	$t_{1/2}$ (min)
600–700	2.24×10^{-8}	19
75–180		7

data very well, with R^2 values of 0.985 and 0.995 for 75–180 μm and 600–700 μm GFH samples, respectively. The average value of the diffusion coefficient is summarized in Table 3. The calculated average value of $\bar{D}$ for arsenic(V) sorption on 75–180 μm and 600–700 μm GFH samples is 2.24×10^{-8} $cm^2 \cdot s^{-1}$. Figure 8 shows that for the smaller GFH particle (75–180 μm), the half time is 7 min, whereas for the larger GFH particle (600–700 μm), the half time is 19 min. The half time for reaching equilibrium is therefore faster for the smaller GFH particles, which indicates that with smaller particles there is an initial larger surface area of GFH to allow for more adsorption of the predominate arsenate ionic species, i.e., $H_2AsO_4^-$ at pH 4. Both the curves on the graph shown in Fig. 8 start to level off after 60 min. Given the high stirrer speed, this would suggest that the slower kinetic performance of bigger size fraction GFH particle (600–700 μm) was mainly due to its pore structure, and the main resistance to the arsenic(V) ion exchange reaction was due to intraparticle diffusion when using the larger particle size fraction. Similar approach was adopted by other researchers to calculate the effective particle phase diffusivity using intraparticle diffusion model (27, 29, 42, 44, 45). We are currently engaged in further studies to improve the kinetic performance of the adsorbents for arsenate sorption and also investigating the effect of other competing anions on As(V) removal from water.

CONCLUSIONS

Pore size distribution results suggest that GFH sample contains significant amount of mesoporosity. The results of pH titration and zeta potential measurements indicate that the difference between PZNPC and IEP for GFH sample is −1.8. This indicates that the internal surface is more negatively charged than the external surfaces. The XRD output of GFH shows considerable amount of crystallinity in the material. It is also evident that GFH sample is not pure as there was a peak associated with hematite (33°). The time of aging the precipitate can be a contributing factor to increased crystallinity. It was also determined that chloride content of GFH sample is

0.60 mmol/g and the equilibrium pH in water is about 3.9. The small pore size of GFH sample indicates the inhibition of chloride removal.

The adsorptive capacity of GFH was found to be high for arsenate. The adsorption of arsenate was found to decrease as the pH of the solution was increased, thus giving the optimal adsorption of arsenate onto GFH in the pH range of 4 with an initial arsenate concentration of 400 μg/L. Langmuir isotherm model was found to be suitable for describing the arsenate adsorption at all pHs. The high adsorptive capacity of GFH for arsenate can be explained by the structure of the GFH, a loose hydrated structure which is permeable to hydrated ions, allowing adsorption to easily occur. The particle size used was also found to have a significant effect on the rate at which the arsenate was adsorbed from solution, as deduced from the kinetic studies. A particle size range of 75–180 μm (diameter) was found to have a better kinetics for arsenate sorption compared to the larger-sized particles in the range of 600–700 μm (diameter), which was evident from the $t_{1/2}$ values of 2 and 19 min, respectively. At a pH of 4, GFH was found to have a greater adsorptive capacity for arsenate in comparison with phosphate. This study indicates that the use of GFH in water treatment would provide a simple and safe method which could easily be utilized by water treatment facilities for the safe removal of this naturally occurring highly toxic material from aquatic environment.

REFERENCES

1. Cullen, W.R. and Reimer, K.J. (1989) Arsenic speciation in the environment. *Chem. Rev.*, 89: 713–764.
2. DeMarco, M.J., SenGupta, A.K., and Greenleaf, J. (2003) Arsenic removal using a polymeric/hybrid inorganic sorbent. *Water Research*, 37: 164–176.
3. Scharfenaker, M.A. (2002) Whiteman's Halloween surprise: 10 μg/l arsenic standard. *J. Am. Water Works Assosc.*, 94 (1): 24–30.
4. 98/83/EC. EC Directive on the quality of water intended for human consumption. *Official Journal of the European communities—Legislation*, 1998, 330 (5/12): 32–54.
5. Ferguson, J.F. and Gavis, J. (1971) A review of the arsenic cycle in natural waters. *Water Res.*, 6: 1259–1274.
6. Kuehnelt, D., Goessler, W., and Irgolic, K.J. (1997). The oxidation of arsenite in aqueous solutions. In *Arsenic: Exposure and Health Effects*; Abernathy, C.O., Calderon, R.L. and Chappell, W.R., eds.; London, 45–54, chapter 4.
7. Penrose, W.R. (1974) Arsenic in the marine and aquatic environments. Analysis, occurrence and significance. *CRC Crit. Rev. Environ. Control*, 465–482.
8. Styblo, M., Del Razo, L.M., Vega, L., Germolec, D.R., LeCluyse, E.L., Hamilton, G.A., Reed, W., Wang, C., Cullen, W.R., and Thomas, D.J. (2000) Comparative toxicology of trivalent and pentavalent inorganic and methylated arsenicals in rat and human cells. *Arch. Toxicol.*, 74: 289–299.
9. Driehaus, W., Jekel, M., and Hildebrandt, U. (1998) Granular ferric hydroxide—a new adsorbent for the removal of arsenic from natural waters. *J. Water SRT Aqua.*, 47 (1): 30–35.

10. Pal, B.N. (2001). Granular ferric hydroxide for elimination of arsenic from drinking water. In *Proceedings of the International Workshop on Technology* BUET-UNU, 59–68.
11. Kartinen, E.O. and Martin, C.J. (1995) An overview of arsenic removal processes. *Desalination*, 103: 79–88.
12. Pierce, M.L. and Moore, C.B. (1982) Adsorption of arsenite and arsenate on amorphous iron hydroxide. *Water Res.*, 16: 1247–1253.
13. Farrell, J., Wang, J., O'Day, P., and Conklin, M. (2001) Electrochemical and spectroscopic study of arsenate removal from water using zero-valent iron media. *Environ. Sci. Technol.*, 35 (10): 2026–2032.
14. Bajpai, S. and Chaudhuri, M. (1999) Removal of arsenic from ground water by manganese dioxide-coated sand. *J. Environ. Eng.*, 125 (8): 782–784.
15. Clifford, D., Sorg, T.J., and Subramonian, S. (1986) Removing dissolved inorganic contaminants from water. *Environ. Sci. Technol.*, 20 (11): 1072–1080.
16. Chwirka, J.D., Thomson, B.M., and Stomp, J.M. (2000) Removing arsenic from groundwater. *J. Am. Water Works Assoc.*, 92 (3): 79–88.
17. Ramana, A. and Sengupta, A.K. (1992) Removing selenium(IV) and arsenic(V) oxyanions with tailored chelating polymers. *J. Environ. Eng.*, 118 (5): 755–775.
18. Shen, Y.S. (1973) Study of arsenic removal from drinking water. *J. Am. Water Works Assoc.*, 65 (8): 543.
19. Sorg, T.J. and Logsdon, G.S. (1978) Treatment technology to meet interim primary drinking-water regulations for inorganics. 2. *J. Am. Water Works Assoc.*, 70 (7): 379–393.
20. Gulledge, J.H. and Oconnor, J.T. (1973) Removal of arsenic(V) from water by adsorption on aluminum and ferric hydroxides. *J. Am. Water Works Assoc.*, 65 (8): 548–552.
21. Sun, X. and Doner, H.E. (1998) Adsorption and oxidation of arsenite on goethite. *Soil Sci.*, 163 (4): 278–287.
22. Johnson, D.L. (1972) Bacterial reduction of arsenate in sea water. *Nature*, 240 (3): 44–45.
23. Driehaus, W., Seith, R., and Jekel, M. (1995) Oxidation of arsenate(III) with manganese oxides in water-treatment. *Water Res.*, 29 (1): 297–305.
24. Vagliasindi, F.G.A. and Benjamin, M.M. (1998) Arsenic removal in fresh and NOM-preloaded ion exchange packed bed adsorption reactors. *Wat. Sci. Tech.*, 38 (6): 337–343.
25. Min, J.M. and Hering, J. (1998) Arsenate sorption by Fe(III)-doped alginate gels. *Water Res.*, 32 (5): 1544–1552.
26. Pourbaix, M. (1966) *Atlas of Electrochemical Equilibria*; Pergamon Press: Oxford.
27. Saha, B., Tai, M.H., and Streat, M. (2003) Adsorption of transition metals from aqueous solutions by modified activated carbons. *Chem. Eng. Res. Des.*, 81: 1343–1353.
28. Oliver, J.P. (1998) Improving the models used for calculating the size distribution of micropore volume of activated carbons from adsorption data. *Carbon*, 336 (10): 1469–1472.
29. Saha, B., Iglesias, M., Cumming, I.W., and Streat, M. (2000) Sorption of trace heavy metals by thiol containing chelating resins. *Solvent Extraction and Ion Exchange*, 18 (1): 133–167.
30. Deliyanni, E.A., Bakoyannakis, D.N., Zouboulis, A.I., Matis, K.A., and Nalbandian, L. (2001) Alkaganeite-type β-FeOOH nanocrystals: Preparation and characterisation. *Microporous Mesoporous Mat.*, 42 (1): 49–57.

31. Crosby, S.A., Glasson, D.R., Cuttler, A.H., Butler, I., Turner, D.R., Whitfield, M., and Millward, G.E. (1983) Surface area and porosities of Fe(III)- and Fe(II)-derived oxyhydroxides. *Environ. Sci. Technol.*, 17 (12): 709–713.
32. Thirunavukkarasu, O.S., Viraraghavan, T., and Subramanian, K.S. (2003) Arsenic removal from drinking water using granular ferric hydroxide. *Water SA.*, 29 (2): 161–170.
33. Fuller, C.C., Davis, J.A., and Waychunas, G.A. (1993) Surface-chemistry of ferrihydrite. 2. Kinetics of arsenate adsorption and coprecipitation. *Geochem et Comochimica Acta.*, 57: 2271–2282.
34. Raven, K.P., Jain, A., and Loeppart, R.J. (1998) Arsenite and arsenate adsorption on ferrihydrite: Kinetics, equilibrium and adsorption envelopes. *Environ. Sci. Technol.*, 32 (3): 344–349.
35. Hingston, F.J., Posner, A.M., and Quirk, J.P. (1971) Competitive adsorption of negatively charged ligands on oxide surfaces. *Discuss. Faraday Soc.*, 52: 334–342.
36. Matis, K.A., Zouboulis, A.I., Zamboulis, D., and Valtadorou, A.V. (1999) Sorption of As(V) by goethite particles and study of their flocculation. *Water Air and Soil Pollution*, 111 (1–4): 297–316.
37. Stumm, W. and Morgan, J.J. (1981). *Aquatic chemistry: An introduction emphasizing chemical equilibria in natural waters*; John Wiley and Sons: New York.
38. Benjamin, M.M. and Leckie, J.O. (1981) Multiple site adsorption of Cd, Cu, Zn and Pb on amorphous iron oxyhydroxide. *J. Colloid Interface Sci.*, 79 (1): 209–221.
39. Ryden, J.C., Syers, J.K., and Tillman, R.W. (1987) Inorganic anion sorption and interactions with phosphate sorption by hydrous ferric-oxide gel. *Soil Sci.*, 38: 211–217.
40. Lumsdon, D.G., Fraser, A.R., Russell, J.D., and Livesey, N.T. (1984) New infrared band assignments for the arsenate ion adsorbed on synthetic goethite α-FeOOH. *J. Soil. Sci.*, 35: 381–386.
41. Jain, A. and Loeppart, R.H. (2000) Effect of competing anions on the adsorption of arsenate and arsenite by ferrihydrite. *J. Environ. Qual.*, 29: 1422–1430.
42. Helfferich, F. (1995). Ion Exchange. Dover Publications Inc.
43. Hwang, Y.L. and Helfferich, F. (1987) Generalized-model for multispecies ion-exchange kinetics including fast reversible-reactions. *React. Polym.*, 5 (3): 237–253.
44. Roy, D., Wang, G.T., and Adrian, D.D. (1993) A simplified solution technique for carbon adsorption model. *Water Res.*, 26 (6): 1033–1040.
45. Najm, I.N. (1996) Mathematical modelling of PAC adsorption processes. *J. Am. Water Works Assoc.*, 8 (10): 79–89.